ALMA Memo 538
Array Configuration Design of the Atacama Compact Array

Koh-Ichiro Morita
National Astronomical Observatory Japan
morita@nro.nao.ac.jp
and
Mark Holdaway
National Radio Astronomy Obaservatory
mholdawa@nrao.ecu

Sep. 15th, 2005

Abstract

In this memo, we present a design concept of the array configuration of the Atacama Compact Array (ACA) and strawperson plan of the configuration design.

Basic parameters of the array configuration of ACA were discussed from the analysis of the sensitivity in *uv* plane of mosaicing observations with the ACA and the ALMA. For detailed design, it was shown that the compact spiral concept is appropriate to meet major requirements for the ACA, which are to obtain higher *uv* response at the short *uv* spacings and better sidelobe performance. To satisfy the sky coverage requirement, the north - south elongation is needed. We propose that the ACA system consists of two configurations, one (Inner Array) is a compact spiral array with small north - south axis ratio ($\times 1.1$) and the other (NS Array) is a dedicated configuration with large north - south axis ratio (~ 1.7). In current actual plan, inner 6 pads are shared by both configurations.

1. Introduction

The Atacama Compact Array (ACA) system is built as a contribution of Japan to the ALMA project, and is designed for use as a part of the entire ALMA system (ASAC 2001, NAOJ 2004). It is composed of an array of twelve 7-m dishes and four 12-m dishes. The 7-m antennas are packed in a very compact configuration to take short baseline data corresponding to the low spatial frequency Fourier components of the brightness distribution of the observed sources. The 12-m antennas are capable of taking single-dish images that contain information of the Fourier components of even lower spatial frequencies (down to zero ideally). These data

are combined with the data from the 64-element array of 12-m antennas in the data processing software to make the final mosaic image of the sources.

The major goal of introducing the ACA system is to enable ALMA to image extended objects with high precision and robustness by direct sampling of the low spatial frequency visiblities at a *uv* gap of the ALMA 64-element array between 6 m and 15 m. For this purpose, it is important to design the system to have sufficient sensitivity at the *uv* gap.

This memo presents the sensitivity distribution in the Fourier plane for the case of mosaicing observations with the 64-element array and the ACA, and shows the importance of the ACA for high fidelity imaging. Then, we discuss the detailed design of the array configuration for the ACA to meet various requirements of the ACA operation. Finally, we propose a strawperson design based on the compact spiral design concept.

2. Basic Requirements

2.1. Sampling of Short UV Spacing

In the image plane, an ideal response (beam pattern or point spread function) of a telescope should have a single smooth peak and no sidelobes like a Gaussian function. If the beam pattern has any sidelobes, they would cause image estimation errors. Deconvolution methods like CLEAN or MEM compensate for deviations from an ideal response (sidelobes), although the deconvolution interacts with thermal noise and calibration errors to result in image errors.

In the *uv* plane, the ideal beam pattern corresponds to a smooth response function similar to a Gaussian function. Large variations of actual *uv* response cause large sidelobes in image plane. As shown in Figure 1, the *uv* response for the most compact configuration of the 64-element array is very close to the desired *uv* response. However, the response dips below the "ideal response" fit curve shortwords of about 13.5 m, and there is no response at all below about 6 m. Even if total power data observed with the 12 m antennas are added, the total *uv* response function has a gap at *uv* range from 6 m to 13.5 m (13.5 m is where the sensitivity of the homogeneous array dips below the ideal sensitivity profile.). Several imaging studies (Morita 2001, Pety 2001, and Tsutsumi 2004) show that such a *uv gap* causes serious degradation of image quality especially for the case of accurate wide field observations.

The major goal of introducing the ACA system is to sample the low spatial frequency visiblities at the *uv* gap directly and to enable ALMA to image extended objects with high precision and robustness. ALMA has a specification that it must make noise-limited images of features down to 0.1 % of the peak brightness. This very demanding specification requires something like the ACA.

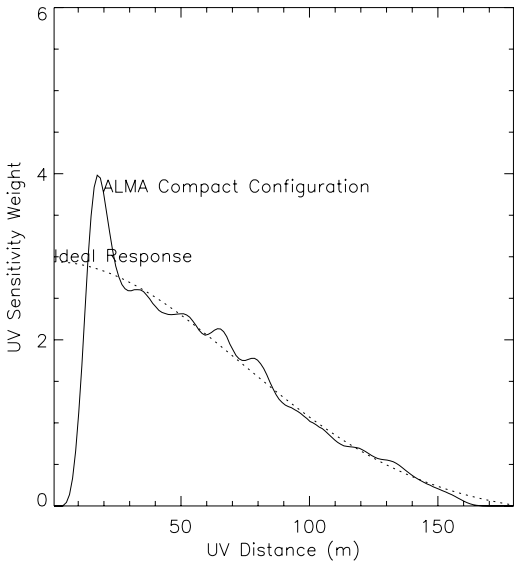

Fig. 1. *UV* response profile, which is similar to a natural *uv* weight profile for the case of mosaic observations, of the moost compact configuration of the ALMA 64-element array for observations with declination of $-23°$ and HA range from -0.25 h to 0.25 h. The exact definition of the *uv* response is described in Section 3.

2.2. Sky coverage

In general, it would be ideal for the ACA to have the same sky coverage as the 64-element array in its compact configuration. The compact NS-elongated array configuration for the 64-element array can cover a declination range from $-85°$ to $40°$ with 55 antennas unshadowed (Conway 2004). Shadowing is also a serious issue for the ACA at declinations outside the range from $-60°$ to $20°$. Elongation of the configuration along the N-S direction or the addition of several pads should be considered for observations of low elevation sources.

2.3. Support for a stand-alone observation

It has been noted that the ACA can also serve as a stand-alone array in a compact configuration at any time for high frequency work (ASAC 2001) and for high fidelity wide-field imaging. For accurate imaging of the ACA stand-alone mode, the synthesized beam pattern of the ACA alone should have reasonably low sidelobes as discussed already for the 64-element array configuration design.

2.4. Accessbility

To make the ACA system very compact, it becomes difficult to access antennas near the array center with a service vehicle. For the case of the antenna transporter, the access area with 12 m $\times$ 30 m should be prepared around antennas according to an ICD (interface control document) between the antenna and the transporter. Since the size of this transporter access

area is very large compared with that of the ACA, if the transporter is not allowed to drive over the ACA antenna pads, it is hard to design the ACA configuration. Therefore, the ACA antenna pads should be designed to allow the transporter to drive over.

For the case of the maintenance of the frontend system, the frontend service vehicle should access every antenna during normal operation. Currently, the vehicle is considered to be similar kind of vehicle to airport high lift trucks, of which width is about 2.5 m. Although the access area definition is not clear in ICD between antenna and the frontend service vehicle at the moment, the rectangular area of 3.5 m $\sim$ 4 m $\times$ 20 m would be needed.

3. *UV* Sensitivity Reponse

In this section, we derive the *uv* sensitivity response function for the combination of the 64-element array and the ACA. This is a similar function to the natural *uv* sampling weight of the single field imaging. In the case of mosaicing observations with the 64-element array and the ACA, we must consider sensitivity differences of baselines and the effect of the mosaicing scan.

3.1. Interferometric Observation

The rms noise level (Jy) of an N element interferometer for a single field observation is given by the equation

$$\sigma_m = \frac{\sqrt{2}kT_{sys}}{\eta A\sqrt{N_{pol}BN_{bl}\Delta t}} \tag{1}$$

where

k : Boltzman constant,
T_{sys} : System Temparature.
η : Total efficiency, which includes antenna efficiency, quantization efficiency, etc,
A : Collecting area of one element antenna,
B : Band width,
N_{pol} : Number of polarization,
N_{bl} : Number of Baselines ($= N(N-1)/2$),
Δt : Integration time.

Equation 1 can be expressed in terms of the single visibility noise $\Delta\sigma_v$ with same bandwidth, same number of polarization, and unit time.

$$\sigma_m = \frac{\Delta\sigma_v}{\sqrt{N_{bl}\Delta t}} \tag{2}$$

The rms noise $\sigma_{\Delta uv}$ for total visibility samples within some *uv* area (Δuv) is defined as same way in image plane, although we need to consider the density variation of uv coverage

of an interferometer. We use the uv sampling density function $S(u,v)$ for expression of uv coverage.

$$N_{bl}t_{obs} = \int_{-\infty}^{\infty}\int_{-\infty}^{\infty} S(u,v)dudv \tag{3}$$

Then, we obtain $\sigma_{\Delta uv}$ in Jy as,

$$\sigma_{\Delta uv} = \frac{\Delta\sigma_v}{\sqrt{\int\int_{\Delta uv} S(u,v)dudv}} \tag{4}$$

From, Equation (4), the noise density $\sigma_v(u,v)$ in uv plane is given by

$$\sigma_v(u,v) = \frac{\Delta\sigma_v}{\sqrt{S(u,v)}} \tag{5}$$

The $\sigma_v(u,v)$ can be also expressed by using the image plane rms noise, σ_m

$$\sigma_v(u,v) = \sigma_m\sqrt{\frac{N_{bl}\Delta t}{S(u,v)}} = \frac{\sigma_m}{\sqrt{S'(u,v)}}, \tag{6}$$

$S'(u,v)$ is the normalized uv sampling distribution as,

$$S'(u,v) = \frac{S(u,v)}{\int_{-\infty}^{\infty}\int_{-\infty}^{\infty} S(u,v)dudv} \tag{7}$$

In general, to obtain the maximum signal to noise ratio in data processings, we use a sampling weight which is a reciprocal of a square of noise. Therefore, we define the uv response function $W(u,v)$ by

$$\begin{aligned} W(u,v) &= \frac{1}{\sigma_v(u,v)^2} = \frac{S(u,v)}{\Delta\sigma_v^2} \\ &= \frac{N_{bl}\Delta t S'(u,v)}{\Delta\sigma_v^2} \end{aligned} \tag{8}$$

$W(u,v)$ is a similar function to the uv natural weight function, which is usually used in noise-limited imaging, and its square root is equivalent to the sensitivity (SNR) in the uv plane.

For mosaicing observations, we have to introduce the mosaicing overlap factor ϵ_m (Holdaway and Rupen 1995). For the case of a rectangular Nyquist grid, $\epsilon_m = 1.60$. Then, rms noise and the sensitivity in the image plane are given by the equations,

$$\sigma_m = \frac{\Delta\sigma_v}{\epsilon_m\sqrt{N_{bl}\Delta t}} \tag{9}$$

For a mosaic field width $= \theta_{mos}$ and total observing time $= t_{obs}$, the observing time for single pointing field Δt is given as

$$\Delta t = t_{obs}/N_p = \alpha t_{obs}/A, \tag{10}$$

where Np is the number of pointings for Nyquist sampling,

$$N_p = \frac{4\theta_{mos}^2}{(\lambda/D)^2}, \tag{11}$$

and

$$\alpha = \pi\lambda^2/(4\theta_{mos}^2) \tag{12}$$

In the case of mosaic observations, the sampling function $S(u,v)$ is no longer a discrete function but the result of convolution of the usual uv coverage with the autocorrelation $a(u,v)$ of the voltage illumination of the element antenna (Cornwell 1988). The normalized uv sampling distribution for mosaic observations can be written as,

$$S''(u,v) = \frac{S'(u,v) * a(u,v)}{\int_{-\infty}^{\infty}\int_{-\infty}^{\infty} a(u,v)dudv} \tag{13}$$

We must also use the mosaicing overlap ϵ_m to calculate the uv noise density for the case of mosaic observations. Then, the uv sensitivity response for mosaic observations is given as

$$W(u,v) = \frac{\alpha\epsilon_m^2 N_{bl} t_{obs} S''(u,v)}{A\Delta\sigma_v^2} \tag{14}$$

3.2. Single Dish Observation

The rms noise in Jy of a single dish measurement is given as

$$\sigma_{sd} = \frac{2kT_{sys}}{\eta_{sw}\eta A\sqrt{N_{pol}B\Delta t}} = \frac{\sqrt{2}\Delta\sigma_v}{\eta_{sw}\sqrt{\Delta t}} \tag{15}$$

where η_{sw} is the switching efficiency of which detailed explanation is shown in ALMA Memo 128 (Holdaway and Rupen 1995). In the same way as the discussion for interferometric case, the uv noise density of a single dish observation is given by

$$\sigma_{sd,v}(u,v) = \frac{\sigma_{sd}}{\sqrt{S'_{sd}(u,v)}} \tag{16}$$

where $S'_{sd}(u,v)$ is an autocorrelation function of a voltage illumination of a main reflector. Therefore, the uv sensitivity weight for a single dish observation will be

$$W_{sd}(u,v) = \frac{\eta_{sw}^2\Delta t S'_{sd}(u,v)}{2\Delta\sigma_v^2} \tag{17}$$

For the case of an observation with N single dishes,

$$W_{sd}(u,v) = \frac{\eta_{sw}^2 N\Delta t S'_{sd}(u,v)}{2\Delta\sigma_v^2} \tag{18}$$

3.3. UV Sensitivity Response of the ACA and the ALMA 64-element array

For mosaicing observations with the ALMA 12 m array, the uv response function is given as follows:

$$W_{alma}(u,v) = \frac{\alpha\epsilon_m^2 N_{bl,alma} t_{obs} S''_{alma}(u,v)}{A_{alma}\Delta\sigma_{v,alma}^2} \tag{19}$$

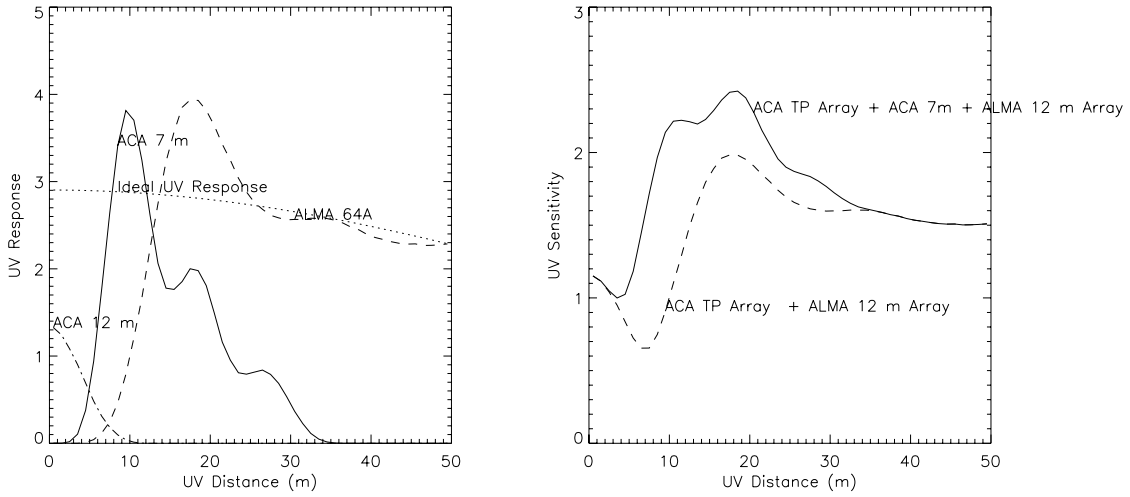

Fig. 2. Left: *UV* response profile of the ACA and the most compact configuration of the ALMA 64-element array with $\beta = 4$. Right: *UV* sensitivity profile. Observing parameters are same as those of Figure 1. The configuration of the ACA is a strawperson design described in Section 7.

If we assume the total integration time of the ACA mosaic observation $t_{obs,aca} = \beta t_{obs}$, then the integration time of a single pointing is

$$\Delta t_{acai} = \alpha\beta t_{obs}/A_{acai} \tag{20}$$

Then, the uv response of the ACA 7 m array (ACAI) is given by

$$W_{acai}(u,v) = \frac{\alpha N_{bl,acai}\epsilon_m^2 \beta t_{obs} S''_{acai}(u,v)}{A_{acai}\Delta\sigma^2_{v,acai}} \tag{21}$$

The uv response of single dish observations with the ACA 12 m total power array (ACAS) is given by

$$W_{sd,acas}(u,v) = \frac{\eta_{sw}^2 \alpha_{acas} N_{acas} \beta t_{obs} S'_{sd,acas}(u,v)}{A_{acas} 2\Delta\sigma^2_{v,acas}} \tag{22}$$

Figure 2 shows the uv reponses of ACA, ALMA 64-element array, and ACA + ALMA 64-element array with $\beta = 4$, and the uv sensitivity (square root of $W(u,v)$) In this caluclation, we assumed that antenna efficiencies of ACA 7m, ACA 12m, and ALMA 12m are same ($\eta_{acas} = \eta_{acai} = \eta_{alma}$). In this figure clearly indicates that, to obtain the total sensitivity response close to the ideal response, we need longer observing time for the ACA than that for the 64-element array to obtain enough sensitivity at the uv gap.

As we already discussed in Section 2, the ACA system is requested to have a similar uv response at the uv gap of the 64-element array to that of the ideal uv response. To indicate how the uv response is close to the ideal one in following design discussion, we used the ratio of averaged responses at the uv gap, γ as follows

$$\gamma = \frac{\int_{UVGAP} W_{acai}(u,v)dudv}{\int_{UVGAP} W_{ideal}(u,v)dudv} \tag{23}$$

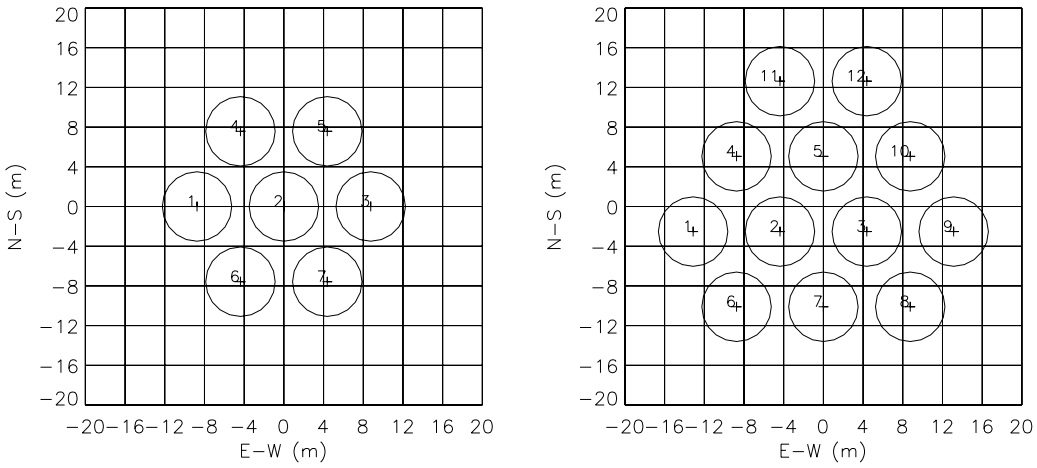

Fig. 3. Triangle Grid Arrays with 7 antennas (left) and 12 antennas (right).

The uv gap area is defined as the area where the $W_{alma}(u,v)$ is less than given threshold level. The uv response at the uv distance less than 15 m results from convolution with autocorrelation $a(u,v)$ of 12 m antenna voltage illumination. Since the low uv response at this area come from contribution of outer area of $a(u,v)$, which often includes errors due to pointing error in actual observations, it would be not appropriate to use very low threshold.

Changing the threshold from 10 % to 30 % does not make much difference in most of cases. In following section, 15 % of $W_{ideal}(u,v)$ was used as this threshold, except for discussion of the antenna packing ratio.

4. Basic Parameters for Array Configuration of the ACA

As we already discussed in Section 2, the ACA system is requested to have a similar uv response at the uv gap of the 64-element array to that of the ideal uv response. In this section, we discuss about the number of antennas of the ACA system requested to obtain such a performance.

Of course, the ratio depends on not only number of antennas but configuration design. In this study, we used the triangle grid type shown in Figure 3, because this type is the most compact. This type of design should be considered an extreme case. Since its sidelobe level is very high, some level of randomization is required to reduce the sidelobe level for actual design. The resultant array configuration would be more sparse and the uv response of resultant array would be reduced.

Figure 4 shows the uv response ratio as a function of the number of antennas with several different diameters. In this calculation, we assumed that the antenna close packing ratio = 1.25. We also assumed the ratio of observing time for the ACA to that of the 64-

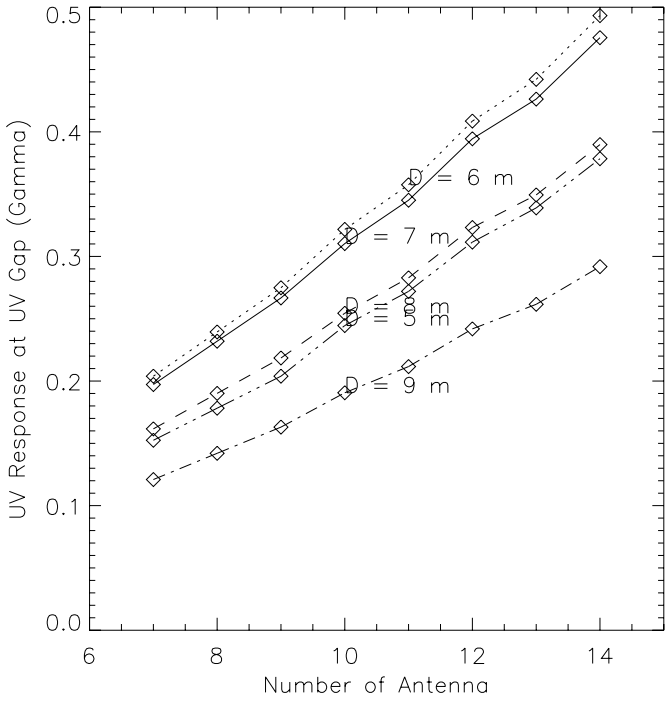

Fig. 4. γ, which is defined by Equation (23), as a function of the number of antennas.

element, $\beta = 1.0$. The figure indicates that γ is in proportion to the number of antennas. On the other hand, for the case of same number of antennas, there is an optimum diameter which gives the maximum uv response. This tendency is easily seen in Figure 5. This figure indicates that the optimum diameter exists the range from 6 m to 7 m, although changing the threshold of the uv gap makes some difference in the results. Since larger antenna has a clear advantage over the antenna calibration, 7 m diameter is suitable selection for the ACA antenna.

Since the uv response is directly proportional to β, a reciprocal of the response ratio $1/\gamma$ indicates requested β to realize the ideal uv response. Figure 4 indicates we will need about 2.5 times more observing time with the ACA than that with the 64-element array for the case of current ACA specification, which is 12 x 7m antennas. In ACA Project Book (NAOJ 2004), the ALMA observing programs that require data taken with the ACA are predicted to comprise no less than 25 % in observing time. Therefore we can adopt $\beta = 4$ for the most possible operation condition. To satisfy this condition, γ in Figure 4 should greater than 0.25 and we need more than 8 antennas for the case of antenna diameter = 7 m. Since, as mentioned above, we have to mitigate the compactness to reduce the sidelobe level, the specification of 12 7 m antennas, of which the margin is about 40 %, is considered suitable for the ACA system.

To reduce the antenna packing ratio is another way to make the array configuration more compact. In Figure 6, we show γ as a function of the antenna packing ratio for the case of 12 antennas. In the case of short uv observations, very small packing ratio is preferable to

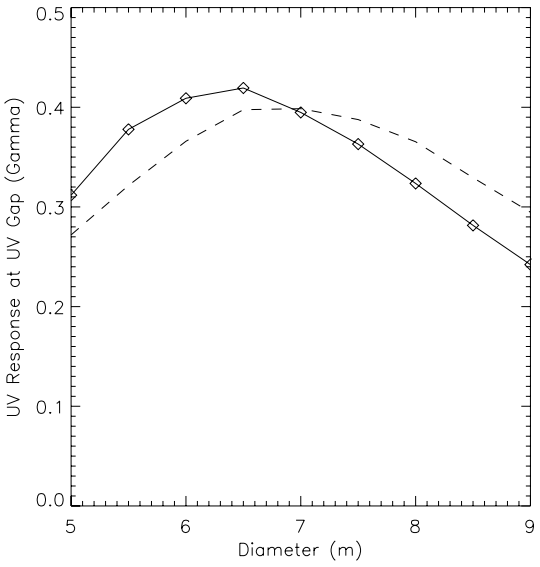

Fig. 5. γ as a function of the antenna diameter for the case of 12 antennas. Solid line: The threshold of the uv gap is 15 % of $W_{ideal}(u,v)$. Broken line: 25 %.

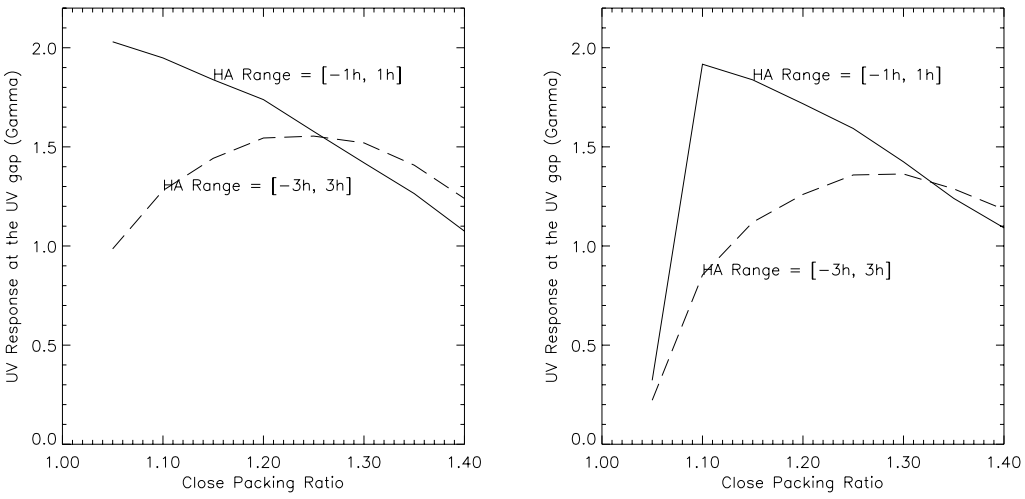

Fig. 6. γ as a function of antenna close packing ratio for the case of 12 antennas. Left: For declination of $-23°$. Right: For declination of $-3°$. In these calculations, we used $\beta = 4$.

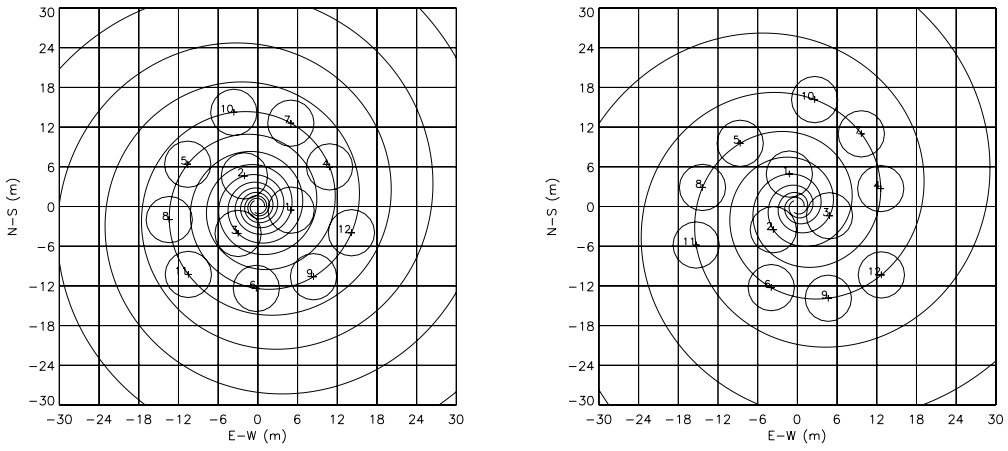

Fig. 7. Examples of the Compact Spiral Configuration. Left figure shows the array configuration with $A = 0.13$. Right shows the confiuration with $A = 0.2$.

obtain high *uv* response at the *uv* gap. However, for the long *uv* track, *uv* response with small packing ratio (< 1.2) reduces drastically due to shadowing effect. Therefore, we can conclude that the packing ratio around 1.25 is good choice to obtain fairly higher *uv* response at the *uv* gap for various observing cases.

5. Compact Spiral Design

5.1. Concept

Compact spiral array is similar kind of configuration to that proposed by John Conway for ALMA configurations (Conway 1998). We can expect a good sidelobe performance with this design, because its *uv* response is to a Gaussian distribution. This is an important factor for the stand-alone imaging. Since the main purpose of the ACA system is to have sufficient uv response at the uv gap, we modified this concept a little to obtain enough *uv* samples at the minimum spacing. We also use 3 logarighmic spirals ($r = exp(A\theta_{AZ})$) start from each antenna of central triangle with the minimum spacing (close packing ratio $\times$ antenna diameter). Then, we put 3 antennas on each spiral with interval of the minimum spacing. Figure 8 shows the relationship between spiral pitch and array dimension by changing the spiral pitch (A in $exp(A\theta_{AZ})$). Examples of the compact spiral array are shown in Figure 7.

5.2. Performance

In Figure 9 we show performances of *uv* response and the sidelobe as a function of the maximum baseline length of the compact spiral. We calculated these performances for various position angles of the array and plotted averaged value. For the *uv* response performance, γ, which is the integrated *uv* response at the *uv* gap normalized by $W_{ideal}(u, v)$, is shown in Figure

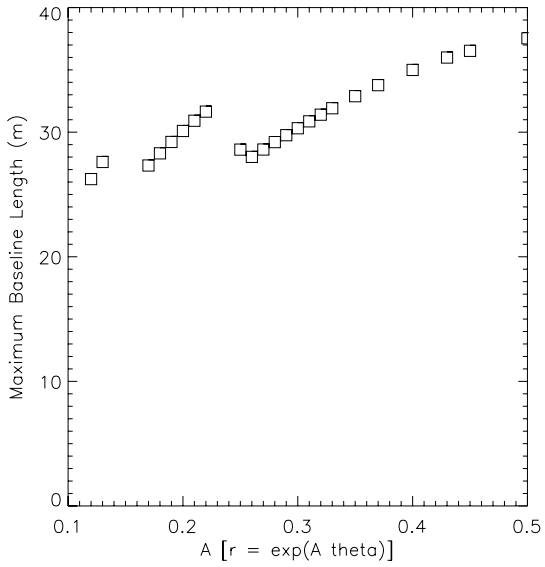

Fig. 8. The maximum baseline of the spiral compact arrray with different pitch angle.

8. We show three kinds of sidelobe performances in this figure; rms near sidelobe, peak near sidelobe, and rms far sidelobe. Near sidelobe area is defined as the area of which distance from the mainlobe is closer to $5 \times \theta_{FWHM}$, where θ_{FWHM} is FWHM of the main beam. We calculated these parameters for observations with Decl $= -23°$, HA range = [-0.25 h, 0.25 h], and $\beta = 1.0$. In Figure 8, we show the performances for the cases of "Triangle Grid Array" and "Circular Array" with 12 antennas as references.

Since Figure 9 indicates that both of γ and sidelobe level are simply in inverse proportion to the maximum baseline length for the maximum baseline range from 26 m to 32 m, it is clear that the optimum configuration which gives high uv response at the uv gap and low sidelobe level simultaneously, are not able to be found easily. If we set desired level of γ, at least rms sidelobe level is almost determined. However, scattering of the peak near sidelobe level is fairly large so that we have some freedom to tune the detailed design. Correlation diagram between the γ and near peak sidelobe level are shown in Figure 10, which indicates that several array configurations (for example A = 0.13 or 0.19) give a faily good performance.

5.3. Accessibility

As shown in Figure 6, there are three open structures at 3 directions between 3 spirals in the configuration of the compact spiral design. It is good characteristics for accessibility to inner antennas. An example is shown in Figure 11.

For this case, the maximum width of the access area of central antennas is determined as a function of the spiral pitch, which is shown in Figure 12 Left. Since the width of the access area is considered to be larger than $3.5 \sim 4$ m, we cannot adopt the array with very small

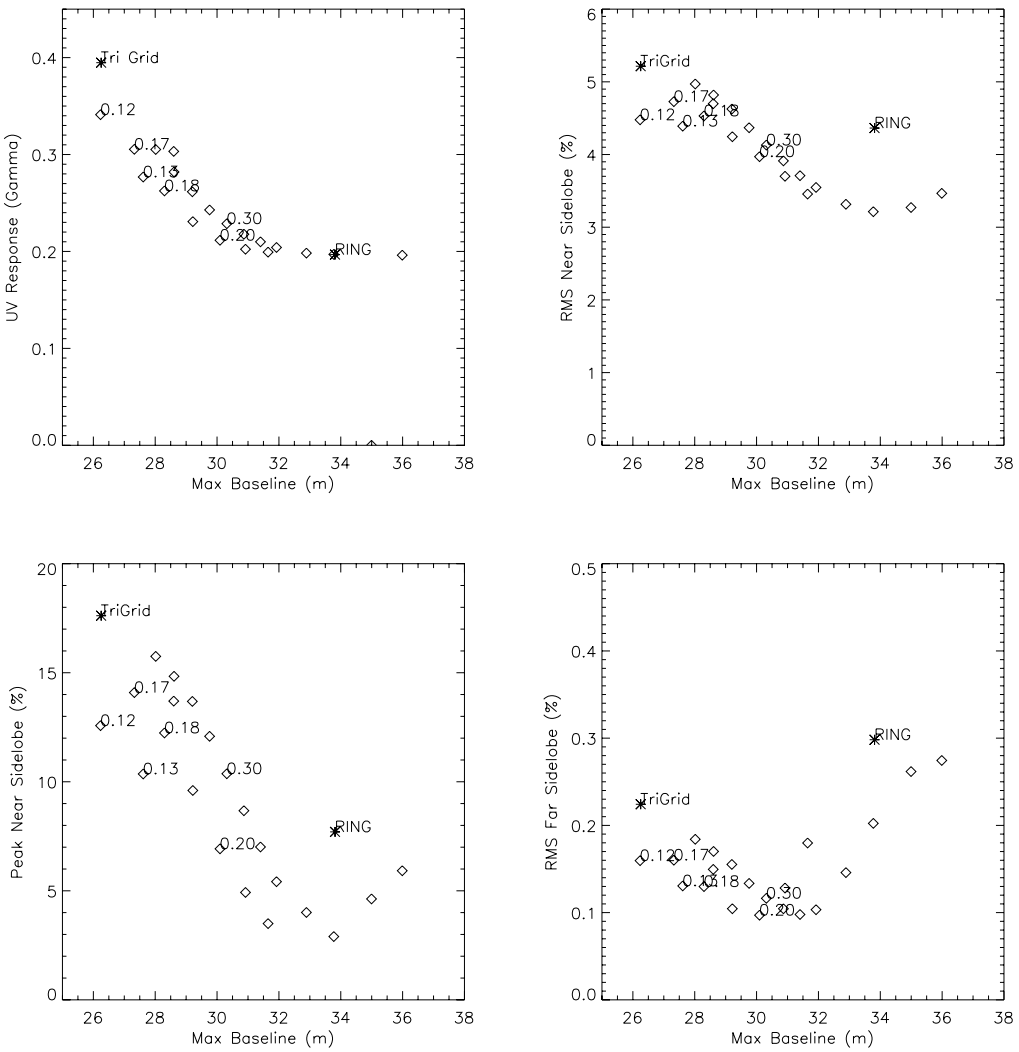

Fig. 9. Performance of the compact spiral array as a function of the maximum baseline for observations with Decl $= -23°$, HA range = [-0.25 h, 0.25 h], and $\beta = 1.0$. **Top left:** γ. **Top right:** RMS near sidelobe level. **Bottom left:** Peak near sidelobe level. **Bottom right:** RMS far sidelobe level. Near sidelobe area is defined as the area of which distance from the mainlobe is closer to $5 \times \theta_{FWHM}$. We also show performnaces with Triangle Grid Array (TriGrid) and Circular Array (RING) in these figures as references.

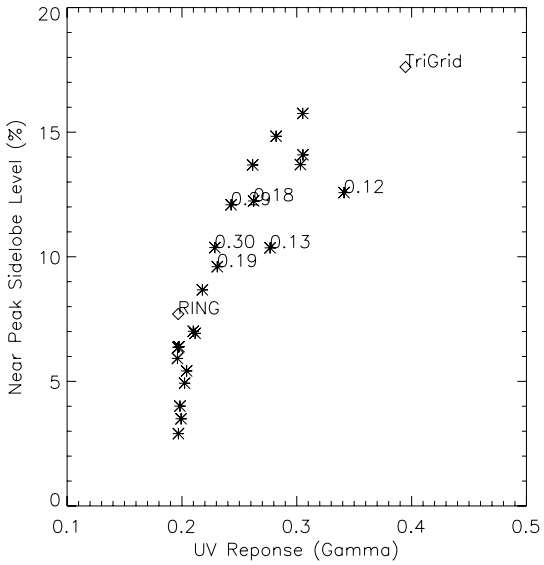

Fig. 10. Correlation diagram between *uv* response (γ) and near peak sidelobe.

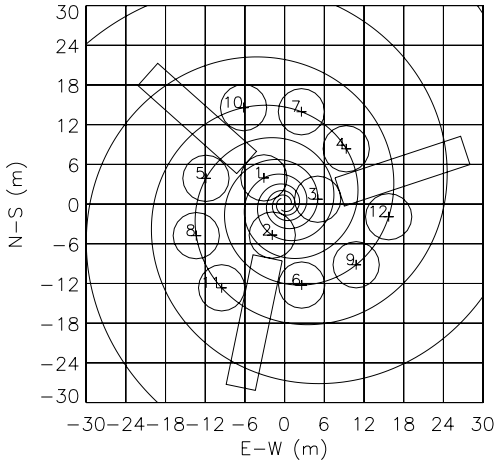

Fig. 11. A layout example of the frontend service vehicle access area.

size ($\sim$ 30 m). Figure 11 *Right*, which the relationship between the maximum width and γ, indicates that we can find a configuration which gives $\gamma > 0.25$, if width of the access area is 3.5 m $\sim$ 4 m.

6. North-South Elongation

The ACA is very compact, so that shadowing effect becomes an issue especially at declinations outside the declination range from $-45°$ to $10°$. As mentioned in section 2.2,

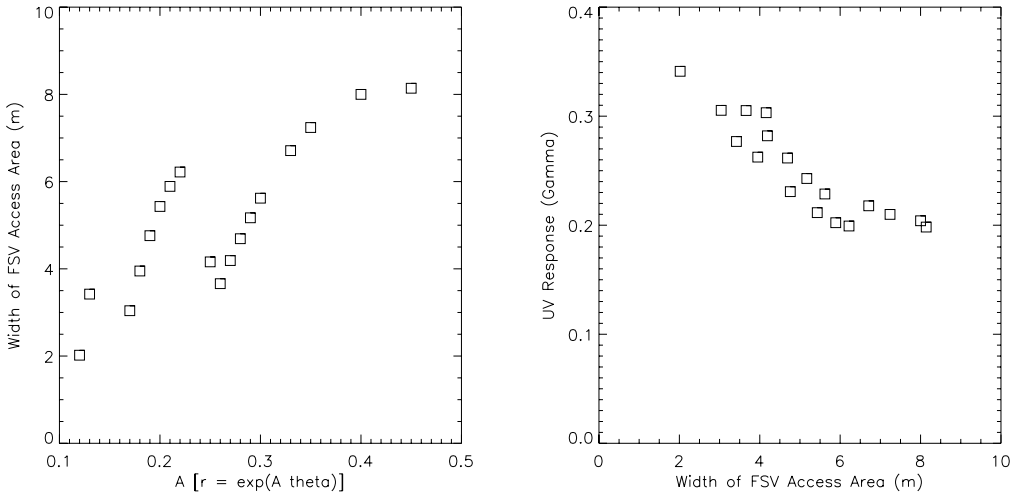

Fig. 12. Left: Width of the frontend service vehicle access area as a functiion of spiral pitch angle. Right: Relationship between the width and the uv response γ.

elongation of the configuration along the north-south direction or the addition of several ppads should be considered for observatiions of low elevation souurces.

Figure 13 shows observing time (hour) of the spiral array of A=0.18 with shadowing loss less than 3 antennas as a function of source declination, which is equivalent to 25 % sensitivity loss. In this figure, observing time for configurations with various north-south axis ratio ("NS Expand" in Figure 12). It is clear that even a slight north - south elongation (~ 1.1) improves the sky coverage of the ACA and the coverage becomes almost from $-60°$ to $20°$. However, to cover extreme declination sources down to $-90°$, or up to $45°$], large north - south axis ratio (¿ 1.7) is required. Dependencies of observing time on the north - south axis ratio are almost similar among different spiral pitch as shown in Figure 14.

On the other hand, the north - south elongation reduces the uv response at the uv gap. Fig. 14 shows γ as a function of the source declination with different north - south axis ratio. In this calculation, we used Conf-1 of John Conway's design (Conway 2004) for intermediate declinations from $-53°$ to $7°$, and Conf-5I $-73°$ to $-53°$ and $7°$ to $27°$. We used Conf-7I for extreme declination range from $-90°$ to $-73°$ and from $27°$ to $47°$. This figure indicates that we can obtain only 50 % of the uv response for the case of the north - south axis ratio of 1.5.

Above discussion suggests that it is not a good idea for the ACA to have a single configuration with a large north - south axis ratio. It is reasonable to have a very compact configuration with small axis ratio for intermediate declination souurces and a dedicated configuration with the axis ratio around 1.7 to accommodate the more extreme declination sources.

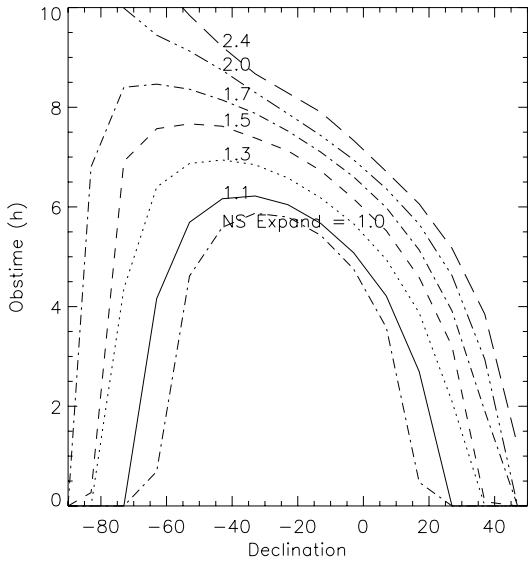

Fig. 13. Observing time (hour) of the spiral array of A=0.18 with shadowing loss less than 3 antennas as a function of source declination. Different north - sourth axis ratio ("NS Expand" in the figure) cases are shown. The shadowing loss less than 3 antennas is equivalent to 25 % sensitivity loss.

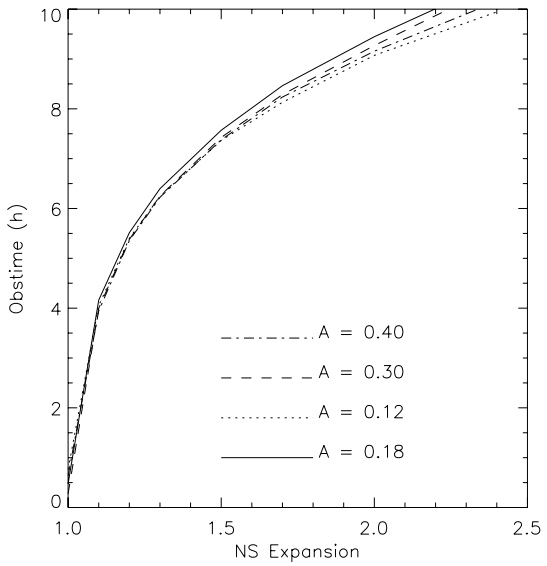

Fig. 14. Observing time as a function of the north - south axis ratio (NS Expand) at Decl = $-53.0°$

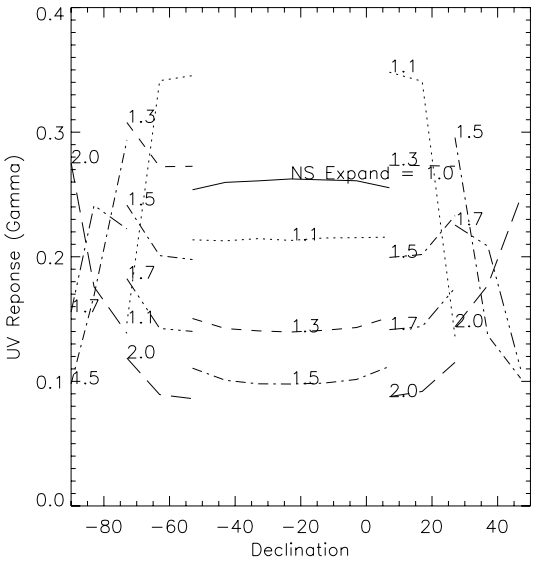

Fig. 15. Integrated uv response at the uv gap (γ) as a function of declination for several north - south axis ratio cases. In this calculation, we used Conf-1 of John Conway's design for intermediate declinations from $-53°$ to $7°$, and Conf-5I $-73°$ to $-53°$ and $7°$ to $27°$. We used Conf-7I for extreme declination range from $-90°$ to $-73°$ and from $27°$ to $47°$.

7. Summary

Important requirements of the ACA array configuration are as follows:

- Sampling of short uv spacing.
- Enough sky coverage.
- Support for a stand-alone observation.
- Accessibility for maintenance.

From uv response analysis, it is found out that at least 12 7 m antennas is required to obtain enough uv sample at short uv spacing. For array type, we showed the compact spiral design is appropriate to meet above requirements. We have examined suitable parameters of this design for the ACA system. To satisfy the sky coverage requirement, the ACA system should have two configurations, one (Inner Array) is a compact spiral array with small north - south axis ratio ($\times 1.1$) and the other (NS Array) is a dedicated configuration with large north - south axis ratio (~ 1.7).

For actual design, it is diffcult to realize two different pad distributions in central crowded area of the ACA site. Therefore, we decided that the central 6 pads are common to Inner Array and NS Array. This design is also desirable to save the pad construction cost. Figure 16 shows a trial design of which A of spiral is 0.18 and the axis ratio of NS Array is 1.7. The left figure shows both of arrays, solid line is pads for Inner Array and broken line is outer pads for NS Array. We show only NS Array pads in the right figure with inner common pads. Resultant

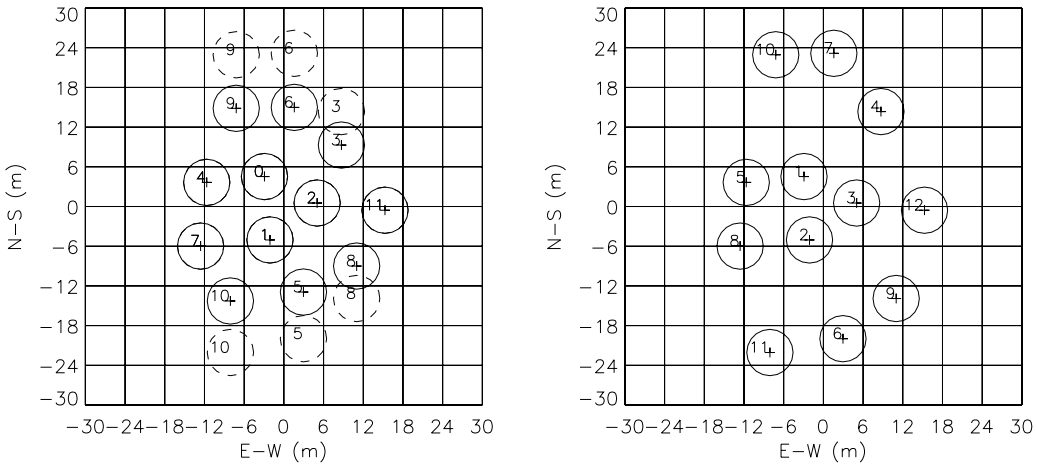

Fig. 16. A trial design for the ACA system. Left: Inner Array (solid line) and NS Array (broken line). Right: NS Array with inner common pads.

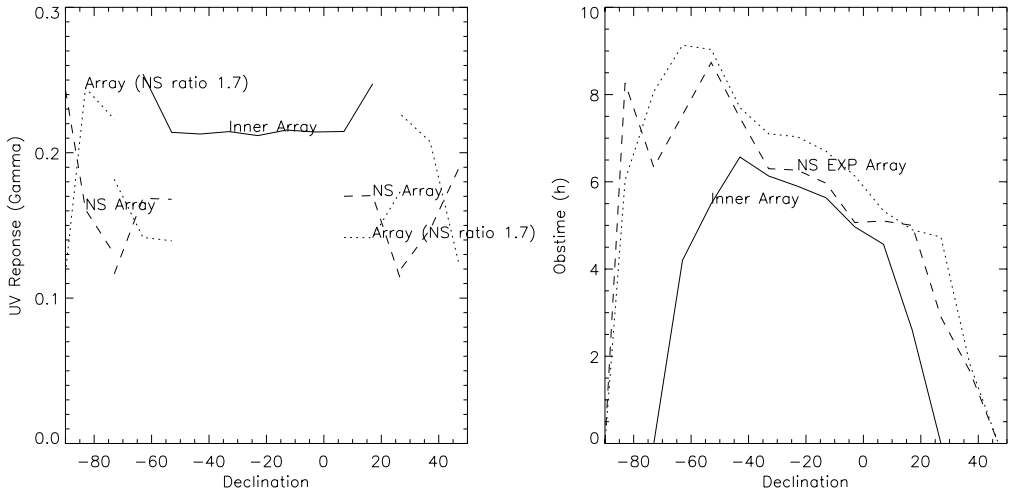

Fig. 17. Performances of a trial array configuration of the ACA system in Figure 16. Left: Integrated *uv* response at the *uv* gap (γ) as a function of declination. Right: Observing time with a shadowing loss less than 3 antennas as a functionn of declination. Solid line is for Inner Array and broken line is for NS Array. Dotted line is for spiral array with $A = 0.18$ and the axis ratio of NS Array is 1.7.north - south axis ratio of 1.7. In the calculationn of γ, we used same array configurations of the 64-element array for the case of Figure 15.

performances are shown in Figure 17.

To complete the design, fine tunings to meet geographical limitation would be needed. Some small randomization of pad position might be also effective.

References

ALMA Science Advisary Committee (ASAC), 2001, "Science Justification for the ALMA Enhancements".

Cornwell, T. J., 1988, "Radio-interferometric Imaging of Very Large Objects", A&Ap, vol.202, 316.

Conway, J., 1998, ALMA Memo 216, "Self-Similar Spiraal Geometries for the LSA/MMA".

Conway, J., 2004, ALMA-90.02.00.00-003-A-SPE, "Antenna Reconfiguration Sequence".

Conway, J., 2004, ALMA-90.02.00.00-001-F-SPE, "Antenna Configurations - Specifications and Requirements".

Holdaway, M. A., and Rupen, M. P., 1995, ALMA Memo 128, "Sensitivity of the MMA in Wide Field Imaging".

Morita, K.-I., 2001, ALMA Memo 374, "Wide Field Immagings with the Atacama Large Millimeter/Submillimeter Array".

National Astronomcal Observatory Japan (NAOJ), 2004, "The Atacama Compact Array System: Project Description".

Pety, J., Gueth, F., and Guilloteau, S., 2001, ALMA Memo 398, "Impact of ACA on the Wide-Field Immaging Capabilities of ALMA".

Tsutsumi, T., Morita, K.-I., Hasegawa, T., and Pety, J, 2004, ALMA Memo 488, "Wide-Field Immaging of ALMA with the Atacama Compact Array: Imaging Simulations".